Synthesis and Reactivity in Inorganic, Metal-Organic, and Nano-Metal Chemistry, 42:121–127, 2012

ISSN: 1553-3174 print / 1553-3182 online
DOI: 10.1080/15533174.2011.609500

Taylor & Francis
Taylor & Francis Group

Structural, Optical, and Magnetic Properties of $MgFe_2O_4$ Synthesized with Addition of Copper

Angappan Sankaramahalingam and John Berchmans Lawrence
CSIR-Central Electrochemical Research Institute, Karaikudi, India

The addition of Cu on the structural, optical, and magnetic properties of $MgFe_2O_4$ prepared by a ceramic technique has been investigated. The Me-O and Me-Me bond lengths increase with the addition of Cu. IR spectra show bands at 540 and 460 cm^{-1}, which confirm Fe^{3+} ions in both tetrahedral and octahedral sites. Room temperature Mössbauer spectra of $MgFe_2O_4$ compounds in zero applied magnetic field show the general trend of increasing hyperfine value and A-B exchange interaction caused by Mg^{2+} ion with Fe^{3+} ions. The addition of copper increases the isomer shift and quadruple splitting of the doublet.

Keywords Cu-added $MgFe_2O_4$, exchange interaction, magnesium ferrite, magnetic properties, oxygen positional parameter

INTRODUCTION

Polycrystalline ferrites are optimal structural materials in high and very high frequency circuits, owing to their excellent electrical and magnetic properties. Moreover, they are more stable than other competing materials, and are able to fulfill a range of applications in radio frequency circuits, operating devices, transformer cores, high-quality filters, choke coils, data storage devices, noise filters, recording heads, antennae, read/write heads for high-speed digital tape, and coil cores.[1–6] Many physical properties of ferrites depend on their microstructure, porosity, grain size, state of chemical order, and the cation distribution,[7–10] and are also strongly connected with the preparative methods.[11] Magnesium ferrite is a soft magnetic n-type semiconducting material that finds application in heterogeneous catalysis, sensors, photoelectrical, and magnetic technologies.[12, 13] The structural formula of magnesium ferrite is usually written as $(Mg^{2+}_{1-x}\ Fe^{3+}_{x})[Mg^{2+}_{x}\ Fe^{3+}_{2-x}]O_4$, where round and square brackets denote cation sites of tetrahedral (A) and octahedral [B] coordinations, respectively, and x represents the degree of inversion, which is defined as the fraction of the (A) sites occupied by Fe^{3+} cations. Interesting physical and chemical properties of ferrospinels arise from their ability to distribute the cations among the tetrahedral (A) and octahedral [B] sites.[7–10] Ladgaonkar and Vaingankar[8] proposed that it is their structural, electrical, and magnetic properties of spinel that determine their applications in many fields. Sepelak et al.[14] studied changes in the structure of $MgFe_2O_4$ caused by high-energy milling using X-ray diffraction (XRD). Rane et al.[15] prepared $MgFe_2O_4$ from synthetic iron oxide obtained from chemically beneficiated iron ore rejects. The cation distribution occurs in such a way that there is not much change in the Fe^{2+}, in spite of the presence of Si, Al, and Mn as impurities. Magnesium ferrite belongs to a partially inverse spinel type, and can be considered as a collinear ferrimagnet whose degree of inversion depends on the thermal history of the sample. The kinetics of formation of $MgFe_2O_4$ was studied by Moustafa and Morsi.[16] The structural and magnetic properties of $MgFe_2O_4$ were determined from transmission electron microscopy, XRD, Mössbauer spectroscopy, and magnetometry by Oliver et al.[17] Narasimhan and Swamy[18] explained interesting variations in cation distribution in solid solutions of composition $MgAl_{2-x}Fe_xO_4$ (x = 0 to 2). Although extensive studies have been performed on the influence of other cations on $MgFe_2O_4$, very limited information is available on the addition of Cu in the ferrite compound. This article reports the results of a study on the structural, optical, and magnetic properties of $MgFe_2O_4$ using XRD, IR absorption spectroscopy, UV-VIS-transmittance spectra, scanning electron microscopy (SEM), and Mössbauer studies.

EXPERIMENTAL

Magnesium ferrite was prepared by a solid-state reaction method using analytical grade MgO and Fe_2O_3 and Cu powder. 10 wt% of Cu was used. The mixture taken in stoichiometric proportions was thoroughly ground to obtain a fine blend, pre-sintered at 900°C for 24 h, and slowly cooled to room temperature. The pre-sintered powders were pelletized in a hydraulic press at 4 T/cm^2 to obtain 1 and 2.5 cm diameter pellets. Then the pellets were sintered at 700°C, 1000°C, and 1300°C for 70 h and furnace-cooled.

Received 21 October 2009; accepted 28 July 2011.
The authors are thankful to the Director, CECRI, and staff of the EPM Division for their support. The authors are grateful to Prof. Ajith Gupta, and Mr. Amit Saraiya of Inter-University Consortium, Indore, for carrying out the Mössbauer measurements.
Address correspondence to Angappan Sankaramahalingam, CSIR-Central Electrochemical Research Institute, Karaikudi 630 006, India. E-mail: angs67@gmail.com

XRD analysis of the ferrite samples were carried out with a JEOL XRD unit (Model 8030) using CuKα radiation (l = 1.54 Å). FTIR spectra of the samples were recorded in the range of 400–1000 cm^{-1} in KBr using a Perkin-Elmer IR spectrometer. UV-transmittance curves were also made using (Varian Carry 500 Scan) UV-VIS-NIR spectrophotometer. Microstructural features were examined using a HITACHI S-3000H Scanning Electron Microscope. Mössbauer spectral measurements were carried out at 298K under an external magnetic field applied perpendicular to the γray direction using a ^{57}Co/Rh γ-ray source. The velocity scale was calibrated relative to ^{57}Fe in Rh.

RESULTS AND DISCUSSIONS

X-Ray Diffraction

Figure 1 shows the XRD patterns of $MgFe_2O_4$ with and without Cu prepared by sintering at 1300°C. The patterns reveal the formation of a single-phase cubic spinel. From the data, the lattice parameter (a), X-ray density (D_x), structure factor F(θ), and oxygen ion positional parameter (u) were calculated and are presented in Table 1. The lattice parameter *a* is calculated from the following relation:

$$a = d\sqrt{(h^2 + k^2 + l^2)} \qquad [1]$$

where *d* is the interplanar distance for the plane *hkl*. The lattice parameter *a* increases with the addition of copper ions, which is attributed to the replacement of smaller Fe^{3+} (0.64 Å) ions by larger Mg^{2+} ions (0.66 Å). A similar behavior was reported for Ti-substituted $Ni_{0.3}Zn_{0.7}Fe_2O_4$, which is neither

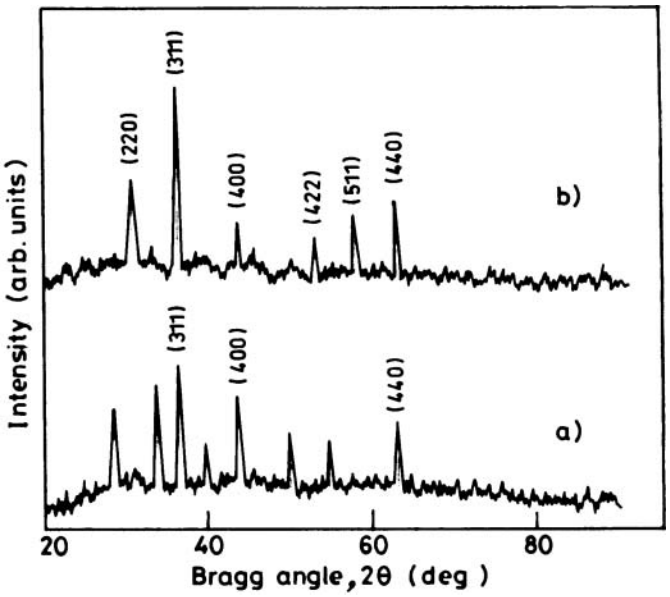

FIG. 1. X-ray diffraction patterns of (a) $MgFe_2O_4$ and (b) $MgFe_2O_4$ + 10 wt% Cu sintered at 1300°C.

TABLE 1
Lattice parameter, x-ray density, structure factor, and oxygen ion positional parameter for $MgFe_2O_4$ compounds

Sample	Lattice parameter a_o (Å)	X-ray density (g/cm^3)	Structure factor F(θ)	Oxygen ion positional parameter (u)
$MgFe_2O_4$	8.352	4.576	1.339	0.431
$MgFe_2O_4$+10 wt% Cu	8.372	4.544	1.411	0.431

a complete normal nor an inverse spinel.[19] The same trend was reported for Ca-substituted $MgFe_2O_4$; it is found that a maximum of 23% of Ca^{2+} can be substituted for Mg^{2+}.[20] The X-ray density (D_x) was calculated using the following formula:

$$D_x = \frac{8M}{Na^3} \qquad [2]$$

where *M* is the molecular weight of the spinel, *N* is the Avogadro number, and *a* is the lattice parameter. The X-ray density decreases with the addition of copper content. This can be ascribed to the density and atomic weight of magnesium (1.74 g/cm^3, 24.31 amu), which are lower than those of iron (7.87 g/cm^3, 55.85 amu) and copper (8.93 g/cm^3, 63.55 amu). The structure factor is a function of oxygen ion positional parameter and distribution parameter (y). The formula for the structure factor for the planes (hkl) are given by Furuhashi et al.[21] The formulae for the multiplicity factor and Lorentz polarization factor are taken from the literature.[22] The oxygen ion positional parameter is calculated by the following equation[23]:

$$u = \left[(r_A + R_0)\frac{1}{\sqrt{3}a} + \frac{1}{4} \right] \qquad [3]$$

From the values it is observed that the lattice parameter and the structure factor are found to increase with the addition of Cu in $MgFe_2O_4$, whereas the X-ray density is found to decrease. The oxygen ion parameter has been found to be equal in both cases. In both cases, the higher octahedral energy for Mg^{2+} ions in comparison to that of Fe^{3+} ions coupled with low oxygen parameter (0.381) accounts for the inverse structure. It may be noted that the oxygen positional parameter is a qualitative measure of the size of tetrahedral sites.[18] The values of oxygen positional parameter for both compounds (0.431) reflect the presence of the same quantity of Mg^{2+} ions at the tetrahedral sites. The values are higher than the reported value (0.381), indicating that the compounds show some deviation from the ideal spinel ferrite. It is due to a gradual increase in Mg^{2+} ions in the tetrahedral sites.[18] In order to determine cation distribution, X-ray intensities were calculated using the following

formula[24]:

$$I_{hkl} = |F_{hkl}|^2 P L_P \quad [4]$$

The distribution of divalent and trivalent cations among tetrahedral and octahedral sites in both ferrite samples are determined from the ratio of intensities of X-ray diffraction lines I_{220}/I_{440} and I_{422}/I_{400}.[25] The intensity of 220 and 422 planes are mostly sensitive to cations on tetrahedral sites[26, 27] and that of 400 planes to the cations in the octahedral sites.[26] The intensity of the 511 plane is sensitive to the oxygen ion parameter.[27] The intensities of the 220 and 422 planes increase with the addition of Cu. This observation reveals that the occupancy of Mg^{2+} ions increases in the A-site. The distances between a cation and its nearest anion[28, 29] and the radius of the tetrahedral and octahedral intensities of the samples were calculated using the following equations, and are presented in Table 2.

$$d_t = a\sqrt{3}(u - 0.125) \quad [5]$$

$$d_0 = a\sqrt{(3u_2 - 2u + 0.375)} \quad [6]$$

$$r_t = d_t - r_0^{2-} \quad [7]$$

$$r_0 = d_0 - r_0^{2-} \quad [8]$$

where r_t and r_o are the radii of the tetrahedral and octahedral intensities, and d_t and d_o are the distances between a cation and its nearest anion.

From the table, it is clear that the occupancy of Mg^{2+}, Fe^{3+} ions in both the A- and B-sites increases with the addition of Cu. The bond lengths between the cations (Me-Me), and anions (Me-O) were calculated using the following relations, and the values are presented in Table 2.

From the table, it is seen that the Me-O and Me-Me bond lengths increase with the addition of Cu. The increase in Me-O and Me-Me bond lengths may be due to the occupancy of increasing amounts of Mg^{2+} ions in the A-site. The increase in Me-O and Me-Me distances may enhance the strength of magnetic interactions on the replacement of magnetic Fe^{3+} ions by non-magnetic Mg^{2+} ions.

FTIR

Figure 2 shows the FTIR spectra of the pure $MgFe_2O_4$ and Cu-added $MgFe_2O_4$. All the samples show two prominent absorption bands ν_1 and ν_2 in the range 540 to 460 cm^{-1}. Band ν_1 is caused by stretching of tetrahedral cation and oxygen bonding, while ν_2 is ascribed to vibrations of oxygen in a direction perpendicular to the axis joining the tetrahedral ion and oxygen. According to Patil et al.[30] band ν_1 originates from intrinsic vibrations of the tetrahedral complexes corresponding to the highest restoring force, while band ν_2 starts from intrinsic bond-bending vibrations of octahedral complexes. It can be seen from the spectra that $\nu_1 > \nu_2$. Furthermore, the absorption bands for the ferrites are found to be in the expected range. The difference in the band positions is due to difference in the Fe^{3+}— O^{2-} distance in the octahedral and tetrahedral configurations.[31] A third band (ν_3) in the spectra is attributed to an Mg^{2+}— O^{2-} complex at the octahedral site. The frequency of band ν_4 depends on the mass of the tetrahedral metal ion complex and hence it is responsible for lattice vibrations of ions at the tetrahedral site. Srivastava and Srinivasan[32] stated that the bond stretching for tetrahedral sites would lead to a higher force constant than that for the octahedral site. The shoulders ν_2" and ν_2"' at 476 cm^{-1} and 449 cm^{-1}, respectively, are assigned to Mg^{2+}— O^{2-} bond in Cu-added $MgFe_2O_4$ synthesised at 1000°C. Splitting of ν_1 and ν_2 into shoulders is not observed for Cu-added $MgFe_2O_4$ at 700°C, which also confirms the absence of excess Fe^{2+} ions.

Me-O		Me-Me	
$p = a(\frac{1}{2} - u)$	[9]	$b = \sqrt{\frac{a}{4}}$	[13]
$q = a(u - \frac{1}{8})\sqrt{3}$	[10]	$c = \frac{a}{8}\sqrt{11}$	[14]
$r = a(u - \frac{1}{8})\sqrt{11}$	[11]	$d = \frac{a}{4}\sqrt{3}$	[15]
$s = \frac{a}{3}(u + \frac{1}{2})\sqrt{3}$	[12]	$e = (\frac{3a}{8})\sqrt{3}$	[16]
		$f = (\frac{a}{4})\sqrt{6}$	[17]

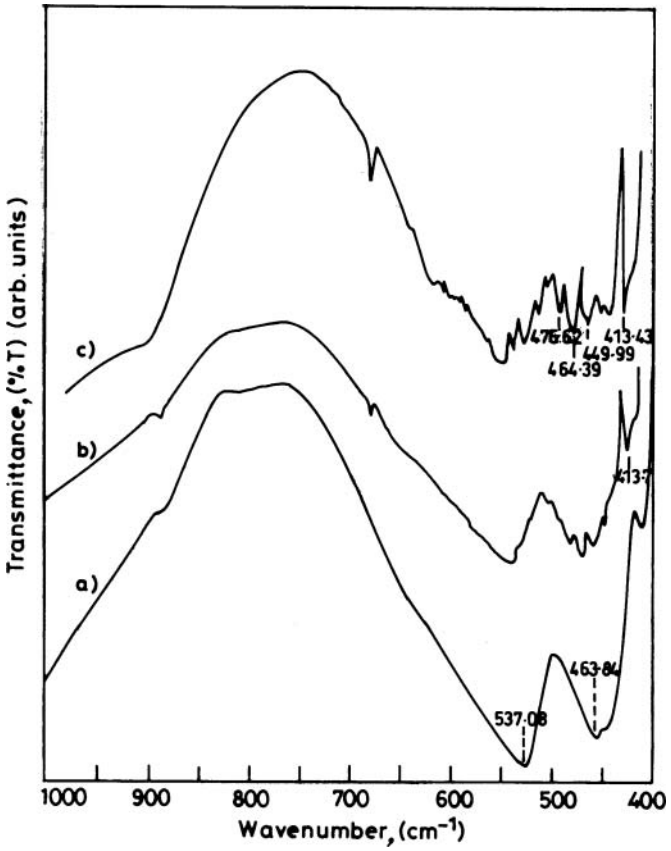

FIG. 2. IR spectra of (a) $MgFe_2O_4$ + 10 wt% Cu sintered at 700°C, (b) $MgFe_2O_4$ sintered at 1000°C, and (c) $MgFe_2O_4$ + 10 wt% Cu sintered at 1000°C.

TABLE 2
Interatomic distances, radii of the tetrahedral and octahedral intensities, and bond lengths between cation-anion (Me-O) and cation-cation (Me-Me)

Compound	d_t (Å)	d_o (Å)	r_t (Å)	r_o (Å)	p (Å)	q (Å)	r (Å)	s (Å)	b (Å)	c (Å)	d (Å)	e (Å)	f (Å)
$MgFe_2O_4$	4.4266	2.2145	3.1066	0.8945	0.58	4.43	8.48	1.73	2.95	3.46	3.62	5.42	5.11
$MgFe_2O_4$ + 10 wt% Cu	4.4372	2.2198	3.1172	0.8998	0.58	4.44	8.50	1.73	2.96	3.47	3.63	5.44	5.13

Similar results have also been reported by Shaikh et al.[33] in the case of Li-Zn-Zr system.

The molecular weights of tetrahedral site (m_t) and octahedral site (m_o) were calculated using cation distribution:

$$\left(Mg^{2+}_{0.44}\ Fe^{3+}_{0.56}\right)\left[Mg^{2+}_{0.56}\ Fe^{3+}_{1.44}\right]O_4$$

Cation distribution in the $MgFe_2O_4$ from X-ray intensity calculations is required for the estimation of the force constants.[34, 35] The force constants of tetrahedral site (k_t) and octahedral site (k_o) were calculated from IR absorption data using the following relations.

$$K_t = 0.04415\upsilon_1^2 M_2\left[\frac{V}{V+3}\right] \quad [18]$$

$$K_o = \frac{0.942128 M_1 \upsilon_2^2}{(M_1+32)} \quad [19]$$

Here $V = \frac{64.2 M_1 u}{M_2}$ and $U = \frac{2K_o}{(\upsilon_1^2 M_1 - 2K_o)}$
where M_1 and M_2 are the molecular weights of the cations on A- and B-sites, respectively. Table 3 summarizes the values of υ_1, υ_2, k_t, and k_o for the samples of $MgFe_2O_4$ with and without addition of Cu. From the table it is observed that the force constants k_t and k_o increase with the addition of Cu as well as with sintering temperature.

TABLE 3
Vibrational frequencies and force constants for $MgFe_2O_4$ compounds

Sample with sintering temperature	υ_1, (nm)	υ_2 (nm)	k_t (dyn/cm^2)	k_o (dyn/cm^2)
$MgFe_2O_4$ + 10 wt% Cu at 700°C	537	463	2.1822×10^5	1.4487×10^5
$MgFe_2O_4$+10 wt% Cu at 1000°C	537	464	2.23×10^5	1.4506×10^5
$MgFe_2O_4$ at 1000°C	539	464	2.1859×10^5	1.4521×10^5

UV Transmittance

The UV-transmittance spectra of the samples were recorded in the wavelength range $200 < \lambda < 1000$ nm, and are presented in Figure 3. The values of absorbance, band edge, and fundamental absorbance edge derived from the figure are presented in Table 4. The fundamental absorption edge (FAE) decreases with the addition of Cu and increases with sintering temperature. This shift in the band edge energy is ascribed to the distortion of the band by lattice interaction.[36] From the linear part of the curve, the extrapolated optical band gap, E_g, for $\alpha = 0$ for each curve was calculated using the following equation:

$$E_g = \frac{1.24}{\lambda} \quad [20]$$

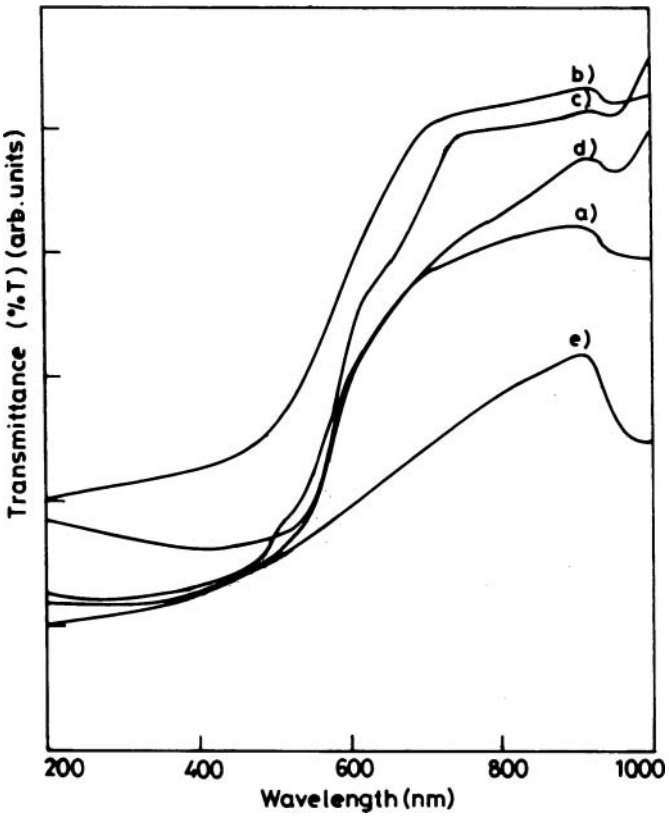

FIG. 3. UV-transmittance spectra of $MgFe_2O_4$ sintered at (a) 700°C; and (b) 1000°C $MgFe_2O_4$ + 10 wt% Cu sintered at (c) 700°C, (d) 1000°C, and (e) 1300°C.

TABLE 4
Absorbance, band edge, and fundamental absorption edge of $MgFe_2O_4$ compounds

Sl.No.	Sample with sintering temperature	Absorpance	Band edge (eV)	FAE (nm)
1	$MgFe_2O_4$ at 700°C	1.2303	2.40	516
2	$MgFe_2O_4$ at 1000°C	1.2589	2.56	484
3	$MgFe_2O_4$+ 10 wt% Cu at 700°C	1.1220	2.46	503
4	$MgFe_2O_4$+10 wt% Cu at 1000°C	1.1482	2.67	465
5	$MgFe_2O_4$ + 10 wt% Cu at 1300°C	1.1220	2.74	452

It is found that the band edge (eV) increases with addition of Cu and also with the increase in sintering temperature. As a result, the band edges shifted from 2.40 to 2.74. For wavelengths above 800 nm, the transmittance of the sample is found to be constant. The percentage transmittance is found to be influenced by the addition of Cu and also by the sintering temperature. It is seen that the FAE decreases with the addition of Cu and also by the sintering temperature, except at 484 nm.

Scanning Electron Microscopy

Figure 4 shows the SEM microstructures of $MgFe_2O_4$ with and without Cu prepared at various sintering temperatures (700, 1000, and 1300°C). The micrographs show that the morphology of the compound is highly influenced by the addition of Cu. The parent compound shows a fine structure with faceted crystallites leaving behind many residual pores. The presence of voids is due to the migration of vacancies from the pore or the neck of the grain boundary. The crystallites are spherical in shape. (Figure 4). Figure 4 reveals the highly dispersed nature of the particles, which appear to aggregate. The duplex structure is formed during the sintering process, with small grain bridges forming around large crystallites. The smaller grains imply that a large number of insulating grain boundaries act as barriers to the flow of electrons. Figure 4 shows the morphology of the sintered Cu-added $MgFe_2O_4$ at 1000°C. The microstructure has a significantly finer grain size, suggesting that the diffusion was impeded when the two phases were well mixed. Figure 4 shows a dense, and homogenous surface with little pores. The average grain size and grain growth seem to have increased with sintering temperature.

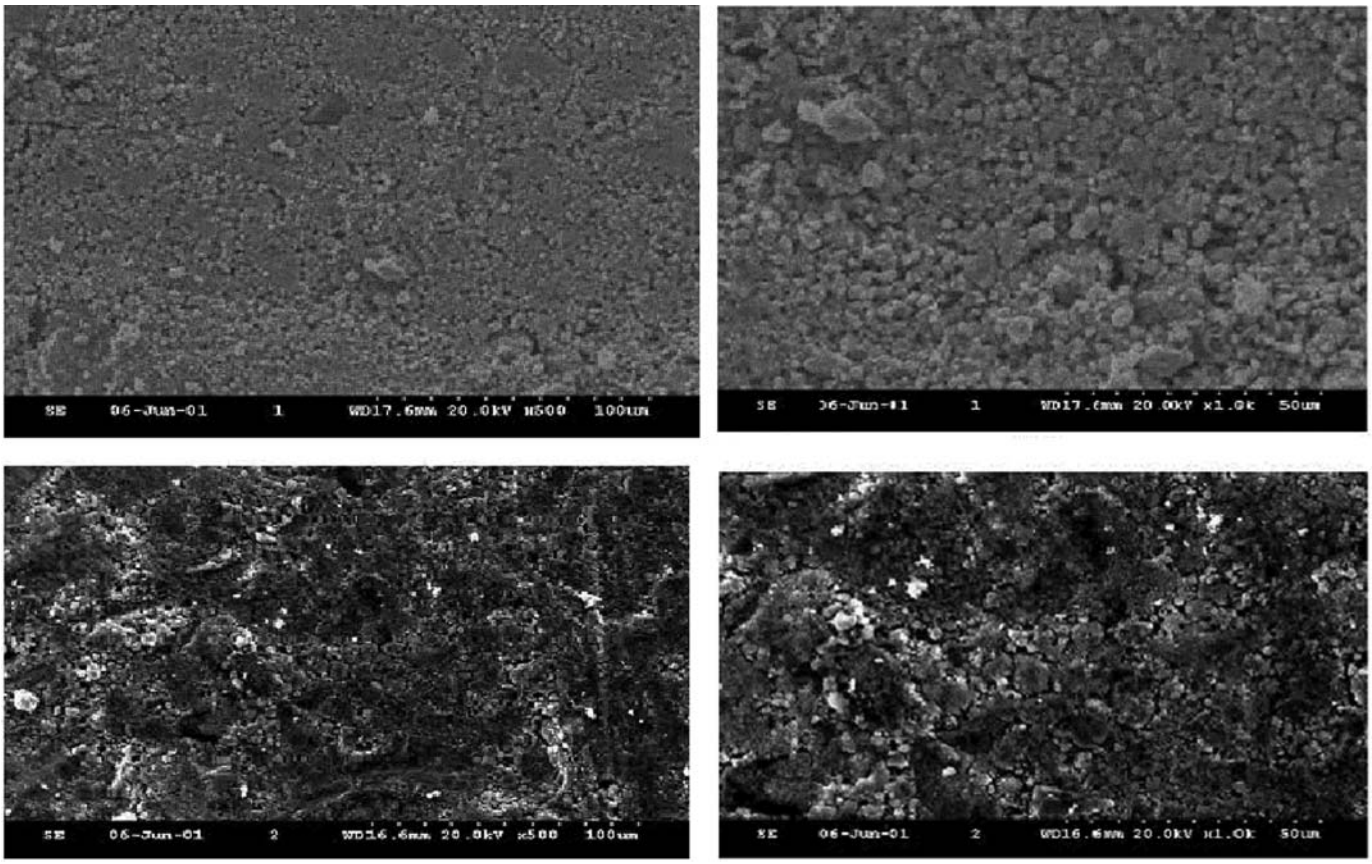

FIG. 4. SEM images of (a) $MgFe_2O_4$; and $MgFe_2O_4$ + 10 wt% Cu sintered at (b) 700°C, (c) 1000°C, and (d) 1300°C.

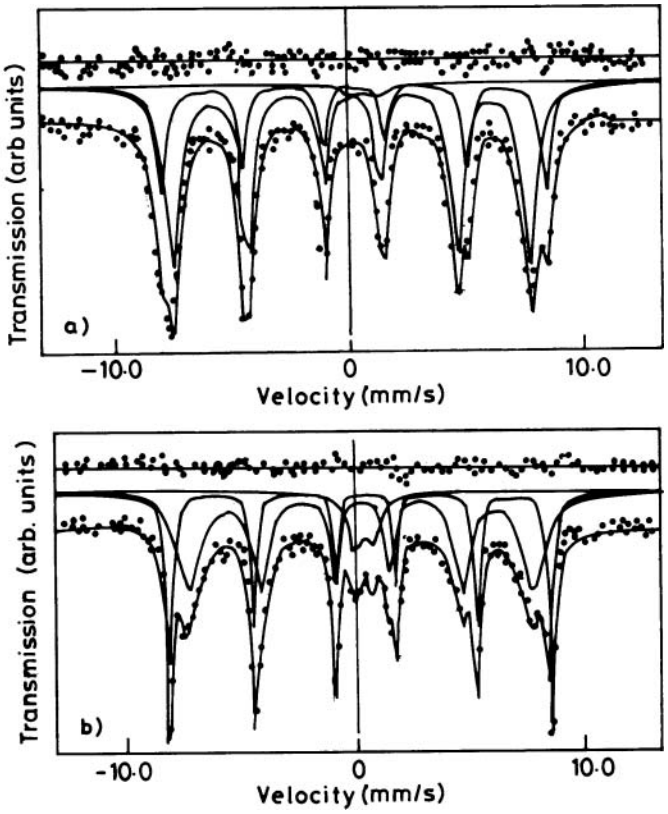

FIG. 5. Room temperature Mössbauer spectra of (a) $MgFe_2O_4$ and (b) $MgFe_2O_4$ + 10 wt% Cu samples sintered at 1000°C.

Mössbauer Spectrum

Room–temperature Mössbauer measurements performed on 1000°C sintered $MgFe_2O_4$ with and without copper are shown in Figure 5. The spectra show two sextets and one doublet absorption. The sextet indicates a magnetic site, while the doublet shows a non-magnetic site. The spectral lines also reveal a partial collapse of the magnetic hyperfine splitting and the appearance of a central doublet (Figure 5). The doublet can be understood to arise from ^{57}Fe in ultrafine ferrite particles exhibiting superparamagnetic behavior.[37, 38] The room-temperature Mössbauer spectrum of $MgFe_2O_4$ was taken at zero applied magnetic field, which indicates that there is a particle overlap of the (A) and [B] sub-spectra due to the smaller difference between the hyperfine fields of the iron atoms in the two sub-lattices. The almost complete resolution of the patterns in the case of $MgFe_2O_4$ is due to octahedrally and tetrahedrally coordinated Fe^{3+} ions. The hyperfine parameters of $MgFe_2O_4$ and Cu-added $MgFe_2O_4$ sintered at 1000° C are presented in Table 5.

The general trend of increase in the hyperfine value is presumably due to the strengthening of A-B exchange interaction caused by Mg^{2+} ions with Fe^{3+} ions.[39] It also indicates that the isomer shifts and the magnetic hyperfine field values are consistent with the high spin Fe^{3+} charge state.[40] The addition of copper increases the isomer shift values from 0.82 to 1.15, which indicates that the s-electron charge distribution of the Fe^{3+} ions changes with the addition of Cu. As indicated, the samples exhibit typical relaxation spectra at room temperature and could be analyzed in terms of the superposition of two sextets and one quadrupole. For the exchange-coupled Fe^{3+} ions in the octahedral sites, it appears that upon addition of Cu there is an overall increase in the hyperfine splitting value from 46.5 to 50.8 in the A-site and 50.1 to 60 in the B-site. This could be due to the relatively strong ferromagnetic exchange interaction with increasing number of Mg^{2+} ions.[39] The degree of inversion, calculated from the sub-spectral area ratio, decreases with the addition of Cu. The sextet with the largest hyperfine field value of 50.1 and the largest center shift is assigned to the Fe^{3+} ions at the B-sites and the sextet with the smallest hyperfine field value of 46.5 and the smallest center shift is assumed to arise from the Fe^{3+} ions at A-sites.[41] Apart from the well-defined sextets, the Mössbauer spectra also consist of a super-paramagnetic doublet whose intensity increases as the particle size decreases. The quadruple splitting of this doublet also increases with the addition of Cu from 0.84 to 1.08. The sextet with the higher isomer shift (IS_A) value of 0.82 and smaller hyperfine splitting (B_{hfA}) value of 46.5 represents the A-site. The sextet with the lower isomer shift (IS_B) value of 0.53 and largest hyperfine splitting (B_{hfB}) value of 50.1 represents the B-site [42]. Thus, each sextet corresponds to Fe^{3+} ions either in A- or B-sites within the fcc array of oxygen atoms.

The Mössbauer spectra of $MgFe_2O_4$ and Cu-added $MgFe_2O_4$ show a small (relative areas of 5% and 9% at the A-site and B-site, respectively) doublet as well as two sextets. Two sextets are observed in the Mössbauer spectra of the inverse spinels due to two environments for Fe^{3+} ions (A-site and B-site), both of which are magnetic due to antiferromagnetic coupling between the two sites. For magnetically ordered spinel ferrites, the magnetic hyperfine field due to Fe at A-sites (B_{hfA}) is

TABLE 5
Hyperfine parameters of $MgFe_2O_4$ compounds

Sample	Isomer shift $IS_{(A)}$ (mm/s)	Isomer shift $IS_{(B)}$ (mm/s)	Area (%)	Hyperfine $B_{hf\,(A)}$ (T)	Hyperfine $B_{hf(B)}$ (T)	Area (%)	QS (mm/s)	Area (%)
$MgFe_2O_4$	0.82	0.53	51	46.5	50.1	44	0.84	05
$MgFe_2O_4$ +10wt% Cu	1.15	0.34	46.9	50.8	60	31	1.08	09

usually smaller (46.5, 50.8) than that of Fe at B-sites (B_{hfB}) (50.1, 60) [43]. The hyperfine fields B_{hf} for the A- and B-sites are determined from the separation between the centroids of the peaks in each Zeeman pattern. The occupation numbers of the Fe^{3+} ions can be considered proportional to the corresponding areas of their Mössbauer spectra. Consequently, the relative numbers of Fe^{3+} ions in the A- and B-sites are determined from the ratios of the areas under the two sub-lattices.[39]

CONCLUSIONS

The influence of Cu addition on the structural, optical and magnetic properties of $MgFe_2O_4$ has been investigated by using XRD, IR absorption spectroscopy, transmittance spectroscopy, SEM, and Mössbauer spectroscopy. The X-ray analysis confirmed the single-phase cubic structure of the samples. The lattice parameter and structure factor were found to increase with the addition of Cu whereas the X-ray density was found to decrease. The oxygen positional parameter has been found to be equal in both the cases. The Me-O and Me-Me bond lengths increase with the addition of Cu due to the increased occupancy of Mg^{2+} ions in the A-site. IR spectral analysis confirms the presence of Fe^{3+}, Mg^{2+} ions on both tetrahedral and octahedral sites. The force constants k_t and k_o are found to increase with the addition of Cu and with sintering temperature due to stretching vibrations of the ions at the tetrahedral and octahedral sites. The optical band gap has been found to increase with the addition of Cu and also with an increase in sintering temperature, whereas the fundamental absorption edge decreases due to the distortion of the band by lattice interaction. The SEM features clearly show that the morphology of the compound is highly influenced by the addition of Cu. Mössbauer studies show an increase in the hyperfine value with the addition of Cu, presumably due to a strengthening of A-B exchange interaction caused by the Mg^{2+} ions with Fe^{3+} ions. The addition of copper also increases the isomer shift values and quadruple splitting of the doublet.

REFERENCES

1. Riches, E.E. A review of materials and applications. In *Ferrites*, Gordon, J. (Ed.), Cook Mills and Boons: London, **1972**, p. 17.
2. Ravindranathan, P.; Patil, K.C. *Mater, J. Sci.* **1987**, *22*, 3261.
3. Igarash, H.; Okazaki, K. *Am. J. Ceram. Soc.* **1977**, *60*, 51.
4. Goldmann, A. *Bull. Am. Ceram. Soc.* **1984**, *63*, 582.
5. Kulikowski, J. *Magn. J. Magn. Mater.* **1984**, *41*, 56.
6. Srinivasan, T.T.; Ravindranathan, P.; Cross, L.E.; Roy, R.; Newnham, R.E.; Sankar, S.G.; Patil, K.C. *Appl. J. Phys.* **1988**, *63*, 3789.
7. Soliman Selim, M.; Turky, G.; Shouman, M.A.; El-Shobaky, G.A. *Solid State Ionics* **1999**, *120*, 173.
8. Ladgaonkar, B.P.; Vaingankar, A.S. In *X-Ray Spectroscopy and Allied Areas*, Joshi, S.K.; Shrivastava, B.D.; Deshpande, A.P. (Eds.), Narosa: New Delhi, **1998**, p. 107.
9. Meenakshisundaram, A.; Gunasekaran, N.; Srinivasan, V. *Phys. Stat. Sol. A* **1982**, *69*, K15.
10. Sankaramahalingam, A.; Lawrence, J.B.; Augustin, C.O. *Tenth National Convention of Electrochemists* (NCE-10), Karaikudi, India, 26–27 April **2001**, p. 18.
11. El Hiti, M.A.; El Shora, A.I.; Hammad, S.M. *Mat. Sci. Tech.* **1997**, *13*, 625.
12. Willey, R.J.; Noirelerc, P.; Busca, G. *Chem. Eng. Commun.* **1993**, *123*, 1.
13. Goldman, A. *Modern Ferrite Technology*. Van Nostrand Reinhold Press: New York, **1990**.
14. Sepelak, V.; Buchal, A.; Tkacova, K.; Becker, K.D. *Mater. Sci. Forum.* **1998**, *278–281*, 862.
15. Rane, K.S.; Verenkar, V.M. S.; Sawant, P.Y. *Bull. Mater. Sci.* **2001**, *24*, 323.
16. Moustafa, S.F.; Morsi, M.B. *Mater. Letters* **1998**, *34*, 241.
17. Oliver, S.A.; Willey, R.J.; Hamdeh, H.H.; Oliveri, G.; Busca, G. *Scripta Metall. Mater.* **1995**, *33*, 1695.
18. Narasimhan, C.S.; Swamy, C.S. *Phys. Stat. Sol. A* **1980**, *59*, 817.
19. Khan, D.C.; Misra, M.; Das, A.R. *Appl, J. Phys.* **1982**, *53*, 2772.
20. Chhaya, S.D.; Pandya, M.P.; Chhantbar, M.C.; Modi, K.B.; Baldha, G.J.; Joshi, H.H. *J. Alloys and Compounds* **2004**, *377*, 155.
21. Furuhashi, H.; Inagaki, M.; Naka, S.N. *Inorg. J. Nucl. Chem.* **1973**, *35*, 3009.
22. Cullity, B.D. *Elements of X-Ray Diffraction*. Addison-Wesley: Reading, Massachusetts, **1956**, p. 302.
23. Standley, K.J. *Oxide Magnetic Materials*. Clarendon Press: Oxford, England, **1972**.
24. Buerger, M.J. *Crystal Structure Analysis*. Wiley: New York, **1960**.
25. Ohnishi, T.T. *Phys, J. Soc. Jpn.* **1961**, *16*, 36.
26. Shenai, V.A. *Tech. of Bleaching and Mercerizing*, 3rd ed. Sevak Publications: Mumbai, **1990**, p. 247.
27. Chidambaram, P.K.; Sreenivasan, S.; Patil, N.B. *Text. Res. J.* **1987**, *57*, 219.
28. Otero Arean, C.; Rodriguez Blanco, J.L.; Rubio Gonzalez, J.M.; Trobajoa Fernandez, M.c. *Mater. J. Sci. Lett.* **1990**, *9*, 229.
29. Shitre, A.R.; Kawade, V.B.; Bichile, G.K.; Jadhav, K.M. *Mater. Letters* **2002**, *56*, 188.
30. Patil, R.S.; Kakatkar, S.V.; Sankpal, A.M.; Sawant, S.R. *Ind. Pure, J. Appl. Phys.* **1994**, *32*, 193.
31. Pradeep, A.; Chandrasekaran, G. *Matt. Lett.* **2006**, *60*, 371.
32. Srivastava, C.M.; Srinivasan, T.T. *Appl. J. Phys.* **1982**, *53*, 8184.
33. Shaikh, A.M.; Bellad, S.; Chougule, B.K. *Magn. J. Magn. Mater.* **1999**, *195*, 384.
34. Ladgaonkar, B.P.; Vaingankar, A.S. *Mater. Chem. Phys.* **1998**, *56*, 280.
35. Ladgaonkar, B.P.; Vasambekar, P.N.; Vaingenkar, A.S. *Ind. Phys. J. A* **2001**, *75*, 351.
36. Hoffmann, H.R.; Martin, S.T.; Choi, W.; Bahnemann, D.W. *Chem. Rev.* **1995**, *95*, 69.
37. Sepelak, V.; Baabe, D.; Litterst, F.J.; Becker, K.D. *Appl. J. Phys.* **2000**, *88*, 5884.
38. Chen, Q.; Rondinone, A.J.; Chakoumakos, B.C.; Zhang, Z. *J. Magn. Magn. Mater.* **1999**, *194*, 1.
39. Kim, C.S.; Lee, S.W.; Park, S.L.; Park, J.Y.; Oh, Y.J. *Appl. J. Phys.* **1996**, *79*, 5428.
40. Van Der Woude, F.; Sawatzky, G.A. *Phys. Rev.* **1971**, *B4*, 3159.
41. Gomes, S.; Francois, M.; Abdelmoula, M.; Retait, Ph.; Pellissier, C.; Evrard, O. *Cement and Conc. Res.* **1999**, *29*, 1705.
42. Bergmann, I.; Sepelak, V.; Becker, K.D. *Solid State Ionics* **2006**, *177*, 1865.
43. Spenser, C.D.; Shroeer, D. *Phys. Rev.* **1974**, *B9*, 3658.